OPEN ACCESS

One-dimensional versus two-dimensional electronic states in vicinal surfaces

New Journal of Physics
The open-access journal for physics

One-dimensional versus two-dimensional electronic states in vicinal surfaces

J E Ortega[1,2,3], M Ruiz-Osés[1], J Cordón[1], A Mugarza[1,4], J Kuntze[2,5] and F Schiller[2]

[1] Departamento de Física Aplicada I, Universidad del País Vasco, Plaza Oñate 2, E-20018 San Sebastian, Spain
[2] Unidad de Física de Materiales CSIC-UPV and Donostia International Physics Center DIPC, Manuel Lardizabal 4, E-20018-San Sebastian, Spain
E-mail: ortega@sq.ehu.es

New Journal of Physics **7** (2005) 101
Received 1 December 2004
Published 29 April 2005
Online at http://www.njp.org/
doi:10.1088/1367-2630/7/1/101

Abstract. Vicinal surfaces with periodic arrays of steps are among the simplest lateral nanostructures. In particular, noble metal surfaces vicinal to the (1 1 1) plane are excellent test systems to explore the basic electronic properties in one-dimensional superlattices by means of angular photoemission. These surfaces are characterized by strong emissions from free-electron-like surface states that scatter at step edges. Thereby, the two-dimensional surface state displays superlattice band folding and, depending on the step lattice constant d, it splits into one-dimensional quantum well levels. Here we use high-resolution, angle-resolved photoemission to analyse surface states in a variety of samples, in trying to illustrate the changes in surface state bands as a function of d.

Contents

1. Introduction 2
2. 1D versus 2D surface states 2
3. Surface states in Au(8 8 7) and Cu(10 10 11) 9
4. Conclusions 13
Acknowledgments 14
References 14

[3] Author to whom any correspondence should be addressed.
[4] Present address: Lawrence Berkeley National Laboratory, University of California, Berkeley, CA 94720, USA.
[5] Present address: Institut für Experimentelle und Angewandte Physik, Olshausenstrasse 40, D-24098 Kiel, Germany.

PII: S1367-2630(05)90627-7

1. Introduction

Surface states of (1 1 1) noble metal surfaces scatter strongly at adatoms, molecules and defects, leading to electron interference phenomena in the surface plane [1]. Surface electron scattering is also noticeable at domain boundaries [2] or monatomic step edges [3]. Steps are particularly attractive for tailoring surface states, since one can easily obtain one-dimensional (1D) patterns with spacings of a few nanometres using vicinal surfaces. These are simply produced by cutting the crystal a few degrees away from the [1 1 1] direction. Although a variety of structures and patterns can be obtained depending on the crystal and the miscut plane and angle (or tilt α), the simplest and most characteristic case is the one schematized in figures 1(a) and (b). Tilting the (1 1 1) surface in the plane perpendicular to the [1 $\bar{1}$ 0] direction usually leads to a 1D array of equally spaced, monatomic, parallel steps of height h, separated by (1 1 1)-oriented terraces of width $w = d\cos\alpha = h/\tan\alpha$. Consequently, macroscopic changes in α, e.g. between 15° and 1°, give rise to 1D superlattices, with nanoscopic lattice constant d between ∼10 and ∼100 Å, respectively.

In the past few years, a number of works have been devoted to the study of surface states in step arrays of Au and Cu surfaces vicinal to the (1 1 1) plane using angle-resolved photoemission spectroscopy (ARPES) [4]–[13] and scanning tunnelling microscopy (STM) [14, 15]. Probably the most interesting observation concerns the change in the dimensionality of the surface state as one varies the superlattice constant d of the step array, as schematically depicted in figure 1. For relatively small d, surface states display electron propagation across the steps, and hence 2D behaviour [4, 5, 7, 8]. In contrast, step arrays with large d lead to weakly dispersing bands, i.e. to strong electron confinement within terraces and quasi-1D quantum levels [6, 9, 10, 12]. In reality, the 1D or 2D nature appears unambiguously defined in surfaces with very large or very small d values, respectively. A less clear behaviour is found for intermediate d values [4, 5], [11]–[14]. A number of different explanations have been given to explain this 1D–2D transition, and all of them lead to similar critical values around $d_c \sim 20$ Å for both Au(1 1 1) and Cu(1 1 1) vicinal surfaces. They include the finite coherence length of the surface state [4], the Fermi wavelength of surface electrons [13] and the onset of overlap with bulk states [4, 5, 7]. The latter is a consequence of the progressive formation of a surface resonance as the projected bulk band gap around the Fermi energy closes [11]. Such surface-state/resonance transition is consistent with STM spectroscopy [14], which nicely reveals the coexistence of mixed 1D–2D components below the Fermi energy in 20–40 Å terraces, as well as with recent theoretical calculations [16].

Here we provide a further insight on surface states of Cu(1 1 1) and Au(1 1 1) vicinal surfaces. First, in section 2 we analyse two extreme cases, i.e. 2D surface states in Cu(3 3 5) with small $d = 8.6$ Å and 1D quantum levels in Au(23 23 21) with large $d = 56$ Å. Later in section 3, we investigate vicinal surfaces with intermediate d values: Au(8 8 7) ($d = 39$ Å) and Cu(10 10 11) ($d = 43$ Å). For Au(8 8 7) one can qualitatively observe the 1D–2D transition, with dispersing bands but relatively large step-potential gaps. The quantitative analysis of the data for the whole set of surfaces is also consistent with a sharp increase in the strength of the confining potential at the step edge at about 40 Å terrace width.

2. 1D versus 2D surface states

The analysis of the complex surface electronic structure of vicinal surfaces requires angle-resolved photoemission combined with synchrotron radiation, thereby providing a thorough

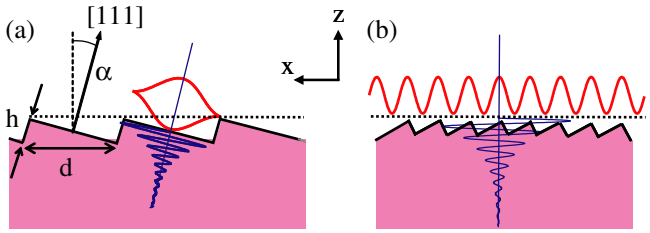

Figure 1. Side view of step arrays of lattice constant d on a vicinal surface of miscut α. (a) For relatively large d, surface electrons get confined within 1D quantum wells (QWs; terraces), whereas (b) for small d, electrons propagate across the step superlattice. The schematic description of the wave function in each case includes the damping tail inside the bulk, which defines a distinct symmetry axis (blue straight line) with respect to the crystal.

description of electron states in the 3D reciprocal space [11]. This includes measuring band dispersion in the direction perpendicular to the steps and analysing the photon-energy dependence of surface bands. Figures 2–6 show the results for Cu(3 3 5) (small d) and Au(23 23 21) (large d). The ARPES experiments have been performed at the PGM beam line in the Synchrotron Radiation Center (SRC) of the UW-Madison, using a hemispherical Scienta SES200 spectrometer. The whole analytical process allows one to obtain, beyond the spectrum of energy levels, the qualitative description of the surface state wave function in both regimes, as depicted in figure 1.

The 1D or 2D character is deduced from the surface band dispersion measured in the direction perpendicular to the step array. In figures 2(a) and 3(a), we show the angle-resolved energy distribution curve (EDC) spectra for Cu(3 3 5) and Au(23 23 21), respectively, which are also shown as intensity plots in figures 2(b) and 3(b). Cu(3 3 5) is vicinal to Cu(1 1 1) with $\alpha = 14.4^\circ$ and $d = 8.6$ Å step lattice constant, and it is characterized by dispersing bands and umklapp replica due to the step lattice. Therefore, in Cu(3 3 5) electron wave functions are 2D extended states of the step array, as in figure 1(b). The umklapp bands reveal electron scattering at step edges. In order to estimate the strength of the step barrier, one can conveniently fit the surface band using a periodic 1D Kronig–Penney (KP) potential model [11]. The latter takes its simplest form by assuming a periodic array of δ-function potentials with barrier strength $U_0 b$, thereby leading to the following dispersion relation:

$$E(k_x) = E_0 + \frac{\hbar^2}{2m^*}\frac{1}{d^2}[\cos^{-1}(|T|\cos k_x d) - \phi]^2, \tag{1}$$

where E_0 is the energy at the band bottom when $d \to \infty$, i.e. for a terrace of infinite width and k_x refers to the wave-vector component parallel to the surface but perpendicular to the steps. $|T|$ is the modulus of the transmission coefficient across the step barrier and ϕ the phase. Both can be expressed as

$$|T|^2 = \frac{1}{1 + (q_0/q)^2} \tag{2}$$

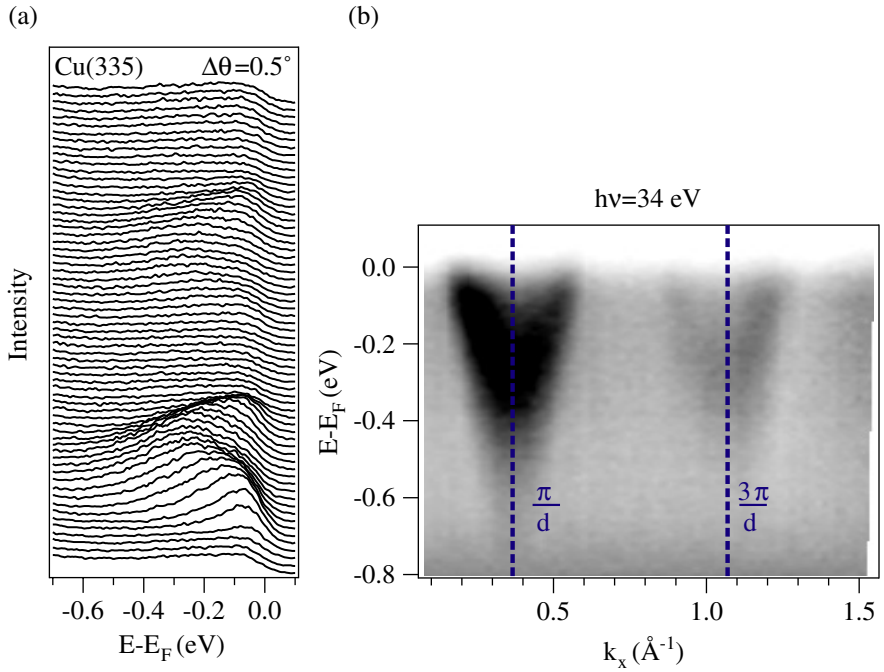

Figure 2. Umklapp bands with $2\pi/d$ step lattice vectors in Cu(3 3 5). The angle-resolved photoemission cascade of spectra in (a) are taken at an increasing emission angle in the direction perpendicular to the step array. Panel (b) is the photoemission intensity plot corresponding to the same data.

and

$$\phi = -\tan^{-1}(q_0/q), \tag{3}$$

where $q_0 = (m^*/\hbar^2) \cdot U_0 b$ and $q = \sqrt{(2m^*/\hbar^2)(E - E_0)}$. For Cu(3 3 5), surface bands cross the Fermi energy, the step-potential gap cannot be observed, and a fit to the complete band is not possible. Yet the barrier strength can be readily estimated from the experimental energy shift $\Delta E = E - E_0$ at the centre of the band with respect to that of the flat surface. From equation (1), substituting the expressions for the transmission probability $|T|^2$ and the phase ϕ, and making $k_x = 0$, we obtain:

$$\Delta E = \frac{\hbar^2}{2m^*}\frac{1}{d^2}\left[\cos^{-1}\left(\frac{1}{\sqrt{1+(q_0/q)^2}}\right) + \tan^{-1}(q_0/q)\right]^2, \tag{4}$$

where q_0 is obtained from this fit and hence the potential barrier $U_0 b$. For Cu(1 1 1) we measure $E_0 = E_F - 430\,\text{meV}$ (see figure 11) and $m^* = 0.41 m_0$, whereas for Cu(3 3 5) we find $E_0 = E_F - 270\,\text{meV}$, and hence $\Delta E = (160 \pm 20)\,\text{meV}$. From equation (4) we obtain $U_0 b = (1.6 \pm 0.2)\,\text{eV Å}$, i.e. a relatively small energy barrier that allows significant electron tunnelling and terrace-to-terrace coupling.

Au(23 23 21) is the most clear example of QW states of terraces measured by ARPES. This surface is vicinal to Au(1 1 1) with a 2.4° miscut and $d = 56\,\text{Å}$ step lattice constant. In the EDC spectra in figure 3(a), we readily detect the presence of three weakly dispersing peaks below

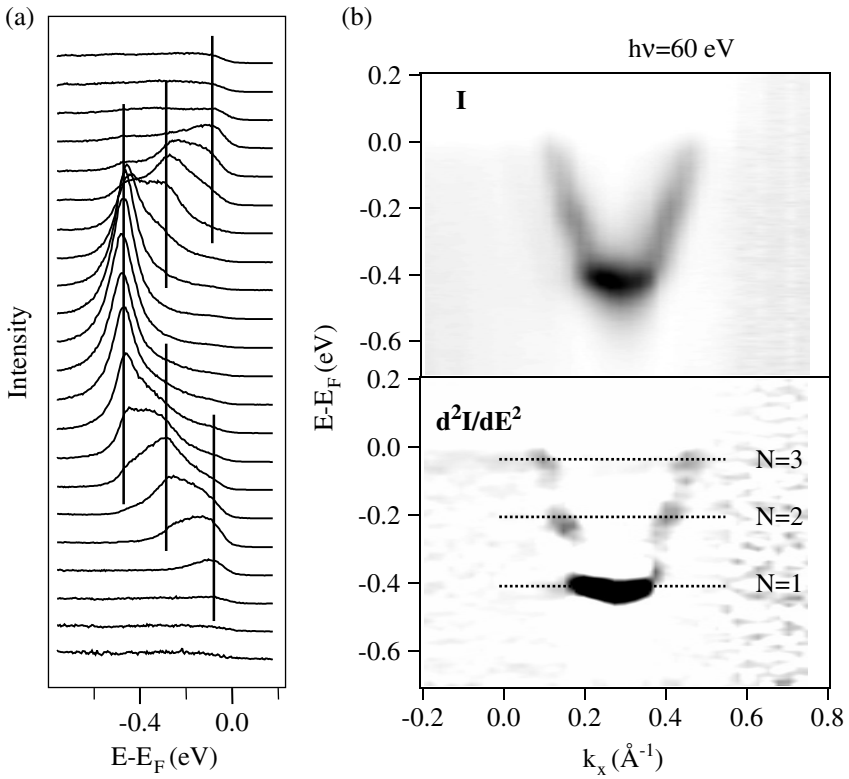

Figure 3. Quasi-1D QW levels of terraces in Au(23 23 21) clearly observed in both the spectrum cascade (a) and the image plot (b). The second derivative in (b) allows one to enhance peak features and minimize the parabolic background from the data [9]. In the image plot, we can observe a tiny dispersion in all quantum levels, which can be used to estimate the minimum barrier strength at the step edge $U_0 b \sim 10\,\text{eV Å}$ [9].

the Fermi energy at $E_F - 430\,\text{meV}$, $E_F - 270\,\text{meV}$ and $E_F - 60\,\text{meV}$. However, we observe a relatively strong parabolic background that obscures the QW peaks in the image plot on top of figure 3(b). The background can be minimized by taking the second derivative of the intensity, as shown in the corresponding image plot at the bottom of figure 3(b) [11]. The nature of this dispersing background, which appears repeatedly in vicinal crystals in the QW regime, has been explained recently as being due to the averaging effect on a surface with significant terrace width distribution (TWD) broadening [13]. However, it can also be a signature of the complexity in both the surface state wave function and the scattering at step edges, as proved by recent STM and ARPES experiments. On the one hand, a distinct 2D surface state band is indeed detected in tunnelling spectroscopy at the same energy of the 2D parabolic background of figure 3, even for the largest terraces [14]. On the other hand, the background becomes weaker as the density of surface steps decreases, as recently shown for stepped Cu(1 1 1) stripes [17].

The relative energy of the non-dispersing peaks of figure 3 with respect to the Au(1 1 1) surface state (at $E_F - 490\,\text{meV}$) and their spectral broadening in the perpendicular direction of the step array (Δk_x) agrees with the three lowest energy levels of an infinite potential well of size $d = 56\,\text{Å}$ [9, 10]. Nonetheless, a closer view of figure 3(b) reveals a weak dispersion along k_x,

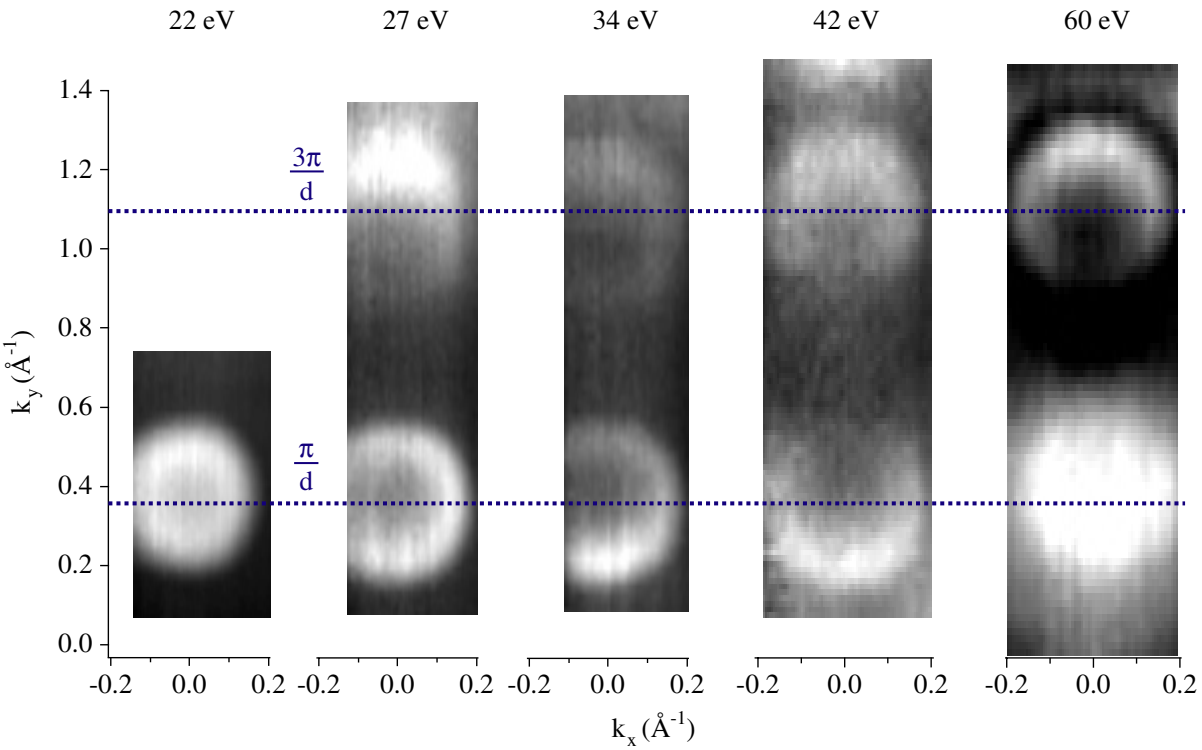

Figure 4. Fermi surface rings in Cu(3 3 5) measured at different photon energies using synchrotron light. The two sets of umklapp rings lie close to the surface Brillouin zone edges and display a photon-energy-dependent intensity.

which can be a combined effect of the small transmission across the step edge barrier and the TWD broadening [9]. Within the 1D KP model of equation (1), the total band width of QW levels in figure 3(b) can be used to estimate the minimum size of the step barrier obtaining $U_0 b = 10\,\text{eV Å}$ [9]. Thus, in Au(23 23 21) steps are significantly large potential barriers that confine electrons, such that these become standing waves inside (1 1 1) terraces, like in figure 1(a).

The schematic description of the electron wave function for both 1D and 2D surface states in figure 1 includes the evanescent part of the surface state, i.e. the exponential tail that decays inside the bulk. It is particularly interesting to observe that this tail defines a distinct symmetry of the wave function with respect to the [1 1 1] direction for 1D or 2D states. Such symmetry can be investigated by tuning the photon energy with synchrotron radiation, as shown in figures 4–6. Figures 4 and 5 display the photon energy dependent Fermi surfaces (FS) for Cu(3 3 5) and Au(23 23 21). k_x and k_y respectively refer to the perpendicular and parallel directions relative to the step array. The ring shape is expected from the 2D character of surface states in Cu(3 3 5). In Au(23 23 21), the ring-like FS results from the combined effect of the spectral distribution of the three quantum levels in figure 3, the TWD and the dispersing background that is visible in figure 3(b) [9]. In both Cu(3 3 5) and Au(23 23 21), we observe two sets of umklapp rings separated by $2\pi/d$ lattice vectors. The relative intensity of the split rings depends on the photon energy, shifting from the first to the second set of rings as the photon energy increases. The photon energy-dependent intensity can be explained as due to the particular Fourier spectrum of the surface state wave function perpendicular to the surface plane.

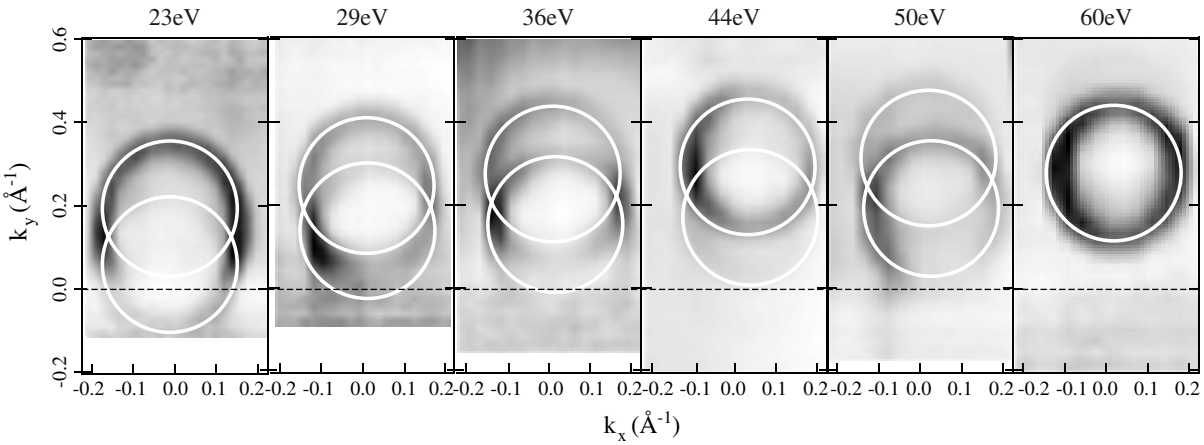

Figure 5. Fermi surface measured by photoemission of Au(23 23 21) as a function of photon energy showing umklapp rings. Due to the larger d value, distances between the Fermi energy circles are considerably smaller than in figure 4.

In fact, by scanning $h\nu$ one probes the different surface state Fourier components that fill up the ΓL line (see figure 7). On the other hand, photoelectron interference effects provoked by the step array lead to similar photon energy dependence, such that one cannot separate both effects [11, 18].

In Cu(3 3 5), the two FS rings are respectively located at the same positions within the surface Brillouin zone (SBZ), i.e. at π/d and $3\pi/d$ ($d = 8.6$ Å), independent of the photon energy. In Au(23 23 21) the location of the FS rings is less clear, although we can appreciate a minor upward shift in both rings along the k_x direction for increasing photon energy. Such a behaviour is more quantitatively analysed in the wave vector plots of figures 6(a) and (b), where k_x positions correspond to the centre of the FS rings of figures 4 and 5, respectively. k_z is obtained from the photoelectron kinetic energy, assuming a free-electron-like final state within the respective $V_0 = 13.5$ and $V_0 = 15.2$ eV inner potentials for Cu(3 3 5) and Au(23 23 21) [11]. For Cu(3 3 5) the two set of data points at π/d and $3\pi/d$ line up perpendicular to the vicinal surface plane, indicating that the surface state Fourier spectrum is broadened along such a direction. This is precisely what we expect for the extended 2D surface state shown in figure 1(b), which appears modulated along the surface plane. For Au(23 23 21), the umklapp sets of (k_x, k_z) points seem not to show a fixed position along the k_x axis, as for Cu(3 3 5), but they rather follow the [1 1 1] direction. Such a behaviour can be explained if the Fourier spectrum is broadened in the direction perpendicular to the terraces, as expected for QW states like those in figure 1(a). However, due to the large uncertainty of the data in the k_x-direction and the proximity of successive $k_x = n\pi/d$ lines ($n = 1, 3, 5, \ldots$), the modulation plane (or wave function symmetry of figure 1) appears less clearly defined in this case.

Figures 2–6 suggest that the changing nature of the surface state on a vicinal surface appears to be related to its wave function properties in the perpendicular direction. It has been recently shown that the surface state wave function becomes very complex in vicinal surfaces due to significant mixing with bulk states locally, around step edges [16]. It is theoretically shown that mixing with bulk states is enhanced as the step density increases. Such a wave function evolution as a function of d can be conveniently understood using the schematic projection shown in

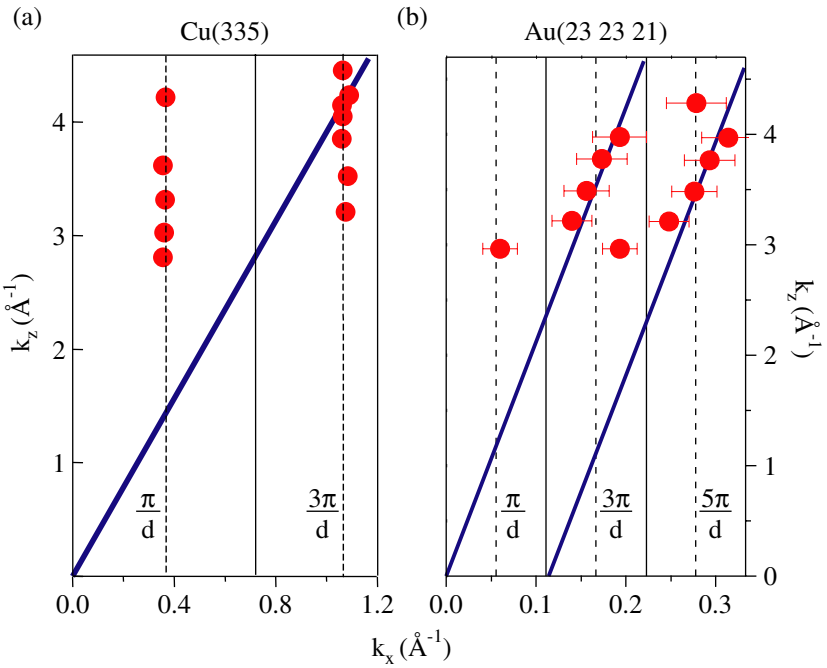

Figure 6. (k_x, k_z) plots for Fermi energy states of (a) Cu(3 3 5) and (b) Au(23 23 21). Data points refer to the centre of the FS rings of figures 4 and 5. In Cu(3 3 5), the points line up perpendicular to the surface plane, whereas in Au(23 23 21) the two umklapp sets appear tilted with respect to the surface normal, lining up close to the [1 1 1] direction. The latter is indicated by the solid blue lines in both cases. These directions would prove a distinct symmetry of the respective wave function with respect to the surface plane, as depicted in figure 1.

figure 7. The circles represent bulk Fermi surfaces (BFS), i.e. constant energy lines at the Fermi level for bulk states. Bulk states project onto the surface plane, which is represented by the thick black line that rotates with the miscut angle. Along this plane, regions of the SBZ where bulk bands are projected from both sides of the BFS are marked in dark grey, whereas regions with projection from only half of the BFS are marked in light grey. The L point projection marks the edge of the SBZ at $\pm\pi/d$. Due to their 2D character, surface states have a broad spectrum along ΓL (thin dotted line). The key point is the overlap between the surface state Fourier components along the ΓL line and projected bulk states at the same energy. On the flat surface of figure 7(a), the bulk projection leaves a gap at $\bar{\Gamma}$, where the entire surface state Fourier spectrum is found. By changing the miscut angle, the surface plane rotates and hence the band projection along the SBZ. At a small miscut, an effective bulk–surface overlap is also possible at the L point via $2\pi/d$ step lattice umklapp [4], as shown in figure 7(b). For larger miscuts, as the projected band gap shrinks, there is an increasing overlap of projected bulk states with surface state Fourier components from L to Γ. At a given miscut, the gap vanishes and the overlap is complete, and hence the surface state becomes a resonance, like in figure 7(c).

The schematic description in figure 7 defines critical α_c values for the onset of bulk–surface state overlap with $k_{neck} \approx 2\pi/d$ ($\alpha_c \approx \tan^{-1}[k_{neck}/2k_{\Gamma L}]$) and gap closing ($\alpha_c = \tan^{-1}[k_{neck}/k_{\Gamma L}]$), when surface states completely become resonances. Here $k_{\Gamma L}$ refers to the ΓL

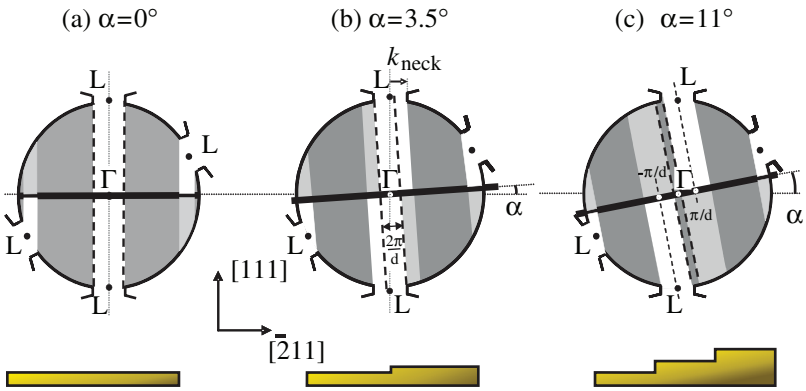

Figure 7. Schematic projection of bulk bands around the Fermi energy for vicinal surfaces with increasing miscut angles α. The $\bar{\Gamma}$ gap of the flat surface in (a) shrinks in (b), and has already vanished in (c). The reducing size of the gap gives rise to a progressive surface–bulk overlap along the ΓL line, where surface states are located. An effective overlap at L can occur via $2\pi/d$ umklapp vectors with even smaller miscuts, as shown in (b).

Table 1. Critical d_c values for the onset of the surface–bulk overlap (via $2\pi/d$ vectors) and the $\bar{\Gamma}$ gap closing calculated at the band bottom from the schematic description of figure 7 for Cu(1 1 1) and Au(1 1 1) vicinal surfaces.

Critical d_c at band minimum	Cu (Å)	Au (Å)
Surface-bulk overlap	33	35
$\bar{\Gamma}$-gap closing	17	18

distance in k-space and k_{neck} to the k-distance between the surface state and the nearest bulk band. The latter depends on the binding energy. Assuming the surface state band in $k_x = 0$ located at $E_F - 490$ meV and $E_F - 430$ meV for Au and Cu crystals respectively, we can obtain the critical terrace widths d_c given in table 1. Thus, we can establish a transition regime for surface–bulk mixing from 35 to 18 Å for Au(1 1 1) and from 33 to 17 Å for Cu(1 1 1). Notice, however, that surface and bulk states can already overlap with smaller miscuts (larger terraces) at the Fermi energy. In fact, due to their larger effective mass, surface states approach bulk band gap edges at E_F, allowing mixing with bulk states with a slight reduction in the gap size of the flat (1 1 1) surface.

3. Surface states in Au(8 8 7) and Cu(10 10 11)

In figures 8–11 we explore the surface state properties for vicinal surfaces with relatively large-step lattice constants d, namely Au(8 8 7) and Cu(10 10 11). The ARPES experiments were performed at 150 K using monochromatized photons of $h\nu = 21.2$, 40.8 and 48.4 eV with mixed s, p-polarization, emitted by a Gammadata VUV 5000 high-intensity He discharge lamp. The spectra were recorded by a Scienta 200 angle-resolved hemispherical analyser, with energy and angular resolutions set to 30 meV and 0.3°, respectively. Cu(10 10 11) and Au(8 8 7) crystals

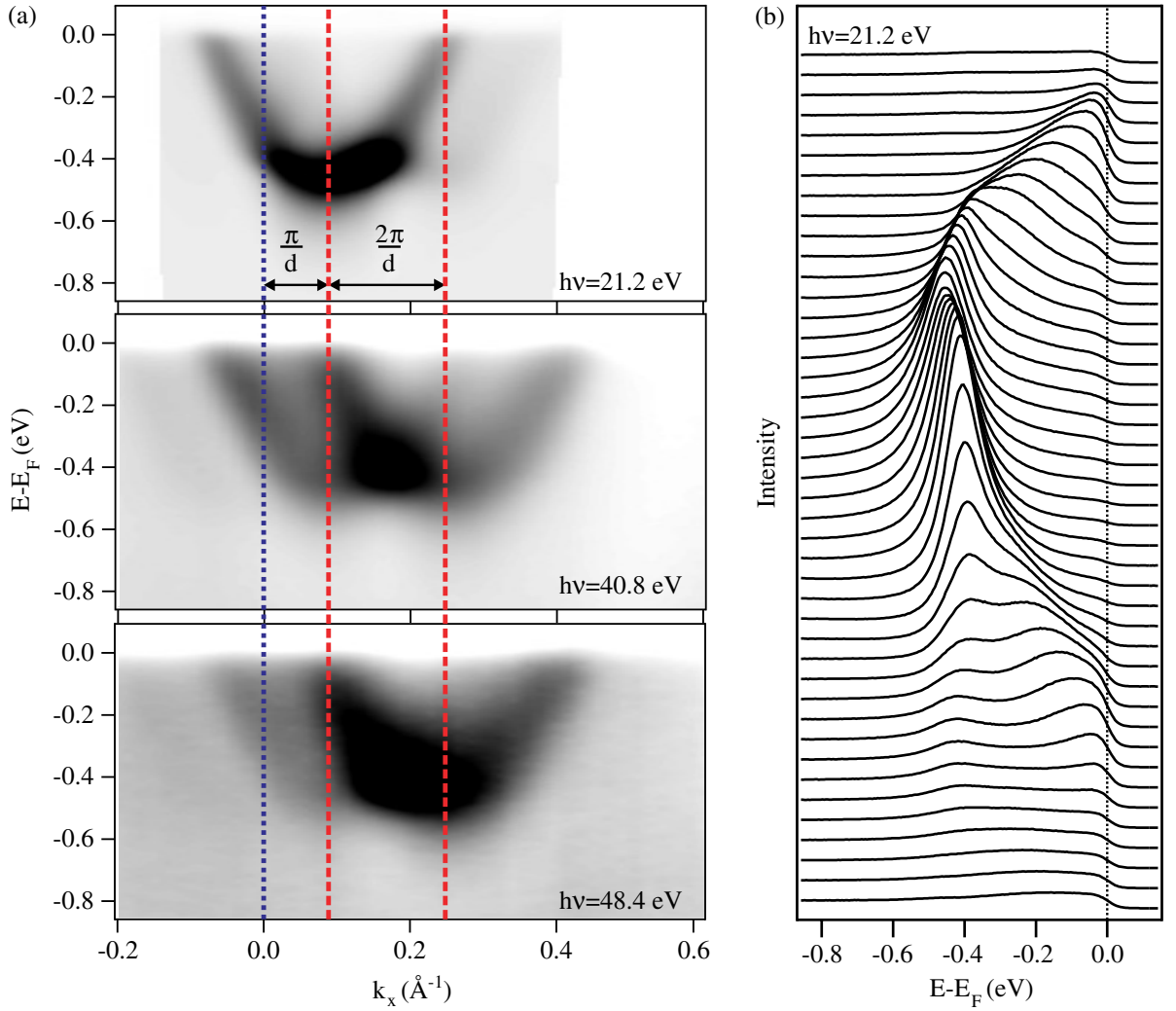

Figure 8. (a) Photoemission intensity plots for Au(8 8 7), taken with monochromatic emission lines from a He lamp. The photon-energy-dependent changes have the same nature as those in figures 2–6. (b) EDC spectra for $h\nu = 21.2\,\mathrm{eV}$, which show two split peaks with smooth dispersion.

have been mounted together with Cu(1 1 1) and Au(1 1 1) surfaces, respectively, such that we can compare surface states of vicinal and flat surfaces measured under the same experimental conditions. This is particularly useful to minimize errors in ΔE.

Figures 8 and 9 display photoemission data for Au(8 8 7). The miscut angle for this surface is $\alpha = 3.5^\circ$ and the step lattice constant $d = 38\,\text{Å}$. The same crystal orientation was already analysed in [6], although using a different sample, lower resolution and synchrotron light with p-polarization. Figure 8(a) shows photoemission intensity plots in a direction perpendicular to the steps for three photon energies, whereas figure 8(b) contains the EDC spectrum cascade for $h\nu = 21.2\,\mathrm{eV}$. The intensity plots display dispersing bands and step superlattice folding effects. The latter actually allows one to obtain a more accurate estimate of the experimental

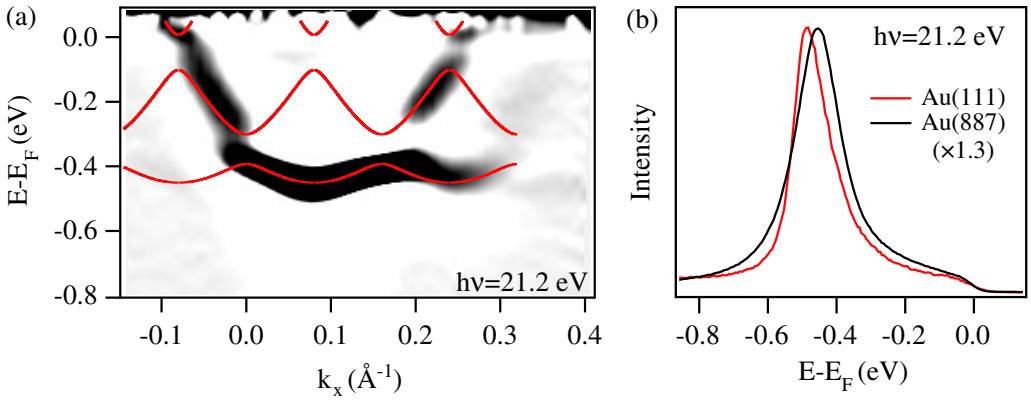

Figure 9. (a) Second derivative image plot for the EDC spectra of figure 8(b). The solid lines are 1D KP bands calculated from equation (1) for a finite $U_0 b = (2.2 \pm 0.5)$ eV Å barrier strength at the step edge. The KP gap between the first two bands (91 meV) is also visible in the image. (b) Surface state spectra from Au(1 1 1) and Au(8 8 7) at their respective band bottoms. Both have been taken under the same experimental conditions and normalized by the Fermi-edge intensity.

lattice constant $d = 39$ Å. The strong superlattice umklapps prove the quality of the step array in this sample. Indeed, due to the herring bone-like reconstruction of (1 1 1) terraces, the Au(8 8 7) surface is characterized by a sharp TWD [6, 11]. In the image plots of figure 8(a), we can observe a strong intensity modulation along k_x, as well as an overall intensity shift to higher k_x as $h\nu$ is increased. Such variations have the same nature as those observed in figures 4 and 5, i.e. they reveal both final state diffraction effects and surface state Fourier composition.

As observed in Au(23 23 21), image plots can hide, within the free-electron-like parabolic backgrounds, a richer band structure. The latter is better observed in both the EDC spectra of figure 8(b) and the corresponding second derivative image plot of figure 9(a). The EDC spectra show two split peaks that follow a smooth dispersion, which is accurately traced in figure 9(a). Earlier experiments carried out for the same surface revealed two non-dispersing QW levels in a direction perpendicular to the steps [6]. In the present case, the improved energy and angular resolution allows one to observe slightly dispersing mini-bands along the SBZ. The solid lines in the second derivative plot represent the 1D KP bands derived from equation (1) that best fit the whole set of mini-bands. As observed in the second-derivative image, a 91 meV energy gap between the lowest two bands is opened. The KP bands have been generated using $m^* = 0.255 m_0$, $d = 39$ Å and $E_0 = E_F - 490$ meV, where the latter binding energy value has been measured for Au(1 1 1) under the same experimental conditions. The KP fit gives $U_0 b = (2.2 \pm 0.5)$ eV Å for the barrier strength, a slightly higher value than those obtained in Au(1 1 1) and Cu(1 1 1) vicinal surfaces with smaller step lattice constants d ([11], see also figure 12).

Figure 10 shows STM and ARPES experiments for Cu(10 10 11). In this case the miscut is $\alpha = 2.6^\circ$ and the step lattice constant $d = 45$ Å. The STM analysis of figure 10(a) indicates a noticeable variation of the terrace width, which is in turn a consequence of the relatively weak step–step interaction in vicinal Cu(1 1 1) [7, 11, 12]. The Gaussian fit to the histogram gives $d = (43 \pm 11)$ Å, and standard deviation $\Delta d/d = 0.25$, i.e., more than double of that obtained

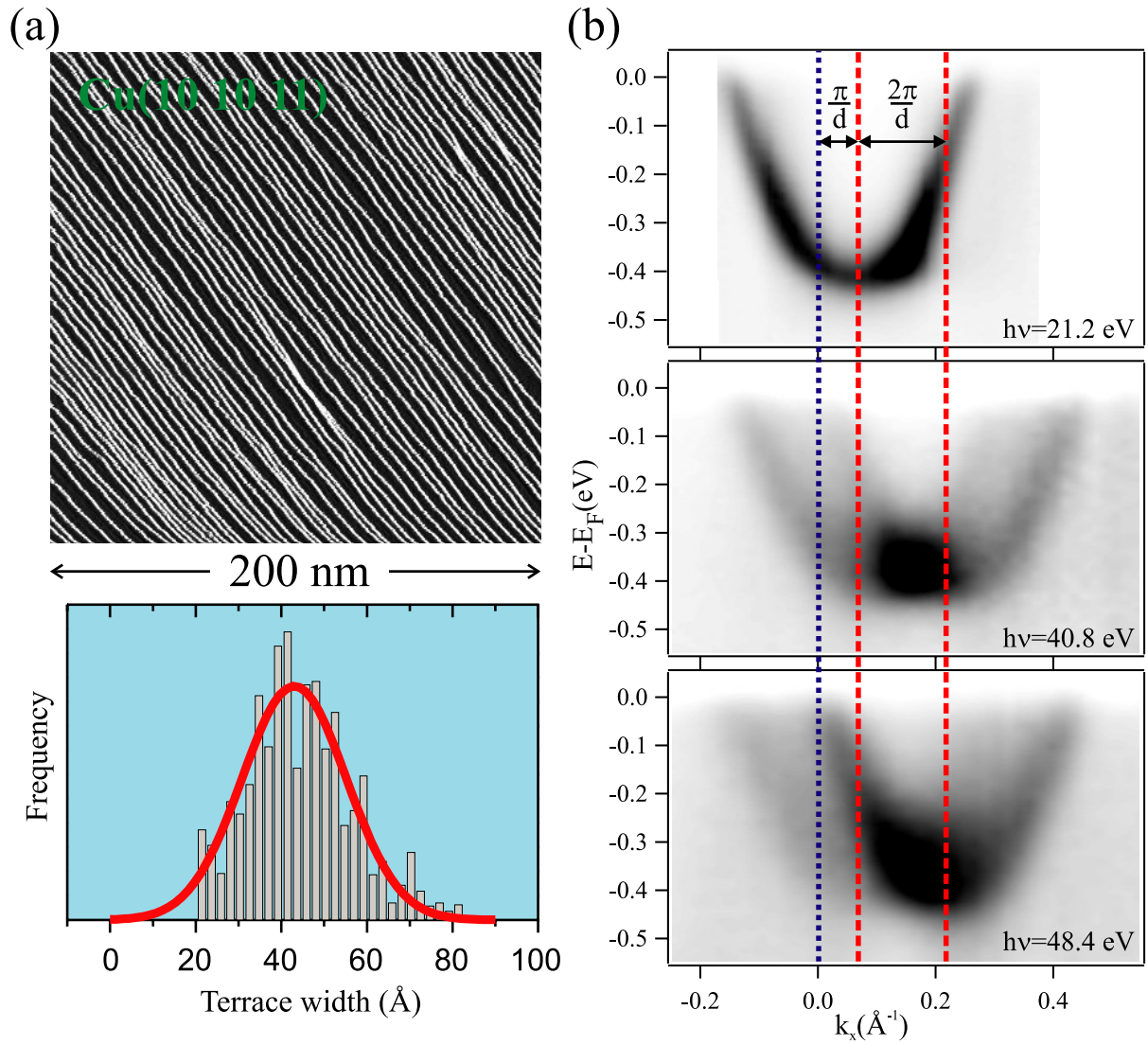

Figure 10. (a) STM image and histogram analysis for Cu(10 10 11). The latter gives a relatively large $\sigma = 0.25$ terrace width broadening. (b) Photoemission intensity plots perpendicular to the steps for Cu(10 10 11) showing parabolic dispersion and photon-energy-dependent band folding with the reciprocal lattice constant d.

in Au(8 8 7) [11]. Although such a large TWD might cause a significant spectral broadening [12, 13], we can still observe weak photon energy-dependent umklapps. However, the second derivative image taken with $h\nu = 40.8$ eV, which is shown in figure 11(a), does not allow one to resolve mini-bands, as in figure 9(a). We can still obtain an estimate of the strength of the confining barrier in Cu(10 10 11) from the shift of the surface band bottom with respect to the flat Cu(1 1 1) surface, as done for Cu(3 3 5). Photoemission spectra at the band bottom for Cu(1 1 1) and Cu(10 10 11) are shown in figure 11(b). The position of the surface state in Cu(10 10 11) is shifted by $\Delta E = (30 \pm 5)$ meV towards the Fermi level, which immediately converts into $U_0 b = (3.0 \pm 1.0)$ eV Å by using equation (4), i.e. higher than Au(8 8 7), but still lower than Au(23 23 21).

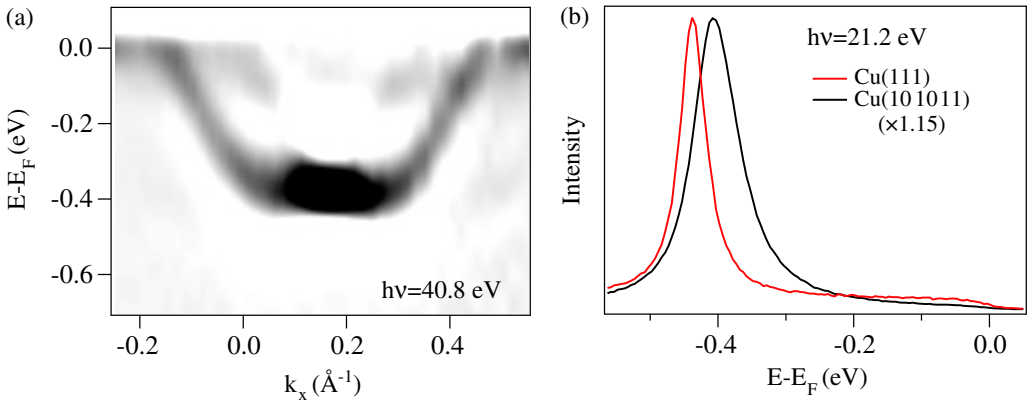

Figure 11. (a) Second derivative image plot for the $h\nu = 40.8$ spectra of figure 10(b). KP bands and gaps cannot be resolved due to terrace broadening. (b) Surface state spectra from Cu(1 1 1) and Cu(10 10 11) taken at their respective band bottoms under the same experimental conditions, and normalized by the Fermi-edge intensity.

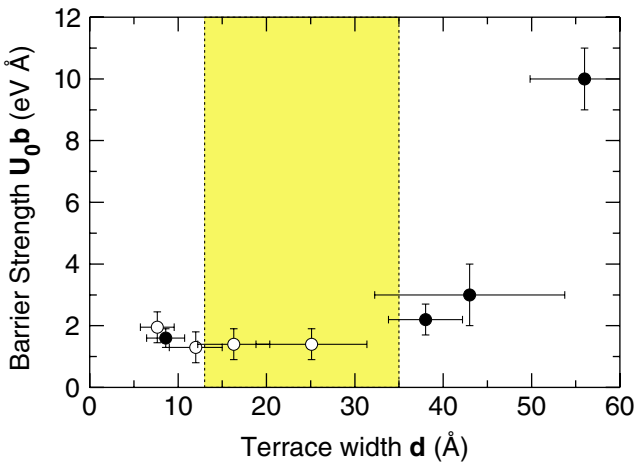

Figure 12. Evolution of the step barrier strength $U_0 b$ as a function of d for Cu(3 3 5), Au(8 8 7), Cu (10 10 11) and Au(23 23 21) (filled circles, from left to right), and Cu(2 2 1), Cu(3 3 2), Cu(4 4 3), and Cu(6 6 5) (open circles, from left to right) taken from [7, 13]. The shaded area marks the surface state/resonance transition region from table 1.

4. Conclusions

Cu(3 3 5) and Au(23 23 21) are two extreme cases of vicinal (1 1 1) noble metal surfaces, revealing 2D surface states and 1D quantum levels, respectively. Au(8 8 7) and Cu(10 10 11) are interesting examples of surfaces with an intermediate step lattice constant. For these two surfaces, high-resolution ARPES experiments display the same overall features of all vicinal surfaces, namely, significant surface band changes with respect to the flat (1 1 1) surface and photon-energy dependent superlattice band folding. Au(8 8 7) clearly displays dispersing bands with relatively

large step-potential gaps. Surface band changes can be analysed within a 1D periodic KP potential giving consistent values of the barrier strength U_0b. In contrast, the photon-energy-dependent analysis is limited to a restricted number of energies, such that the wave function symmetry with respect to the surface plane, as defined in figure 1, cannot be properly determined.

The evolution of the step barrier as a function of d is shown in figure 12 (filled circles) for the different cases analysed in this work. The open circles correspond to U_0b values for Cu(2 2 1), Cu(3 3 2), Cu(4 4 3) and Cu(6 6 5), directly determined from the band bottom shift (equation (4)) with respect to Cu(1 1 1) at 300 K, and using data from [7, 12, 13]. The uncertainties in U_0b are connected to the TWD in each case (error bars in the horizontal axis). For the literature data, we have assumed a constant $\sigma = 0.25$ as the standard deviation [7, 11, 12]. For Au(23 23 21) we represent the minimum barrier strength, as explained before. The shaded area of the figure indicates the surface-state-to-bulk resonance transition region calculated in table 1. Within the error bars, we observe a minimum value of U_0b in the middle of such a transition region. Around this transition region, the barrier displays a slight increase for smaller d and a sharp rise beyond $d = (35–40)$ Å. The increasing barrier strength for high-step densities, which has been also shown in previous analysis [11], might not have physical sense. At very large miscut angles, the surface state is expected to evolve towards the $\bar{\mathrm{M}}$ surface state of the (1 0 0) surface ($\alpha = 55^\circ$) near E_F [19, 20], and it is entirely determined from the features of the L-neck gap projected at $\bar{\mathrm{M}}$ [21]. On the other hand, the barrier strength significantly increases for $d > 40$ Å, i.e. beyond the edge of the transition region at ∼35 Å. However, we notice that TWD-related error bars enter the shaded area for both Au(8 8 7) and Cu(10 10 11), such that data points for these surfaces are partially located beyond the surface–bulk mixing threshold of table 1. Taking this into account, figure 12 generally proves the projection scheme in reciprocal space depicted in figure 7, i.e. the step barrier changes due to the progressive overlap between surface and bulk states.

Acknowledgments

This work was supported by the Spanish Ministerio de Ciencia y Tecnología (MAT2002-03427,MAT-2002-11975-E,HA2002-0107), the Universidad del País Vasco (1/UPV/EHU/00057.240-EA-13668/2001), the DAAD/MCyT exchange program and the European Science Foundation. We thank F J Himpsel and the staff at the Synchrotron Radiation Center (SRC) for beam line support. The SRC is funded by the National Science Foundation (award no DMR-0084402).

References

[1] Heller E J, Crommie M F, Lutz C P and Eigler D M 1994 *Nature* **369** 464
Hla S W, Braun K F and Rieder K H 2003 *Phys. Rev.* B **67** 201402
[2] Chen W, Madhavan V, Jamneala T and Crommie M F 1998 *Phys. Rev. Lett.* **80** 1469
Bürgi L, Brune H and Kern K 2002 *Phys. Rev. Lett.* **89** 176801
[3] Crommie M F, Lutz C P and Eigler D M 1993 *Nature* **363** 524
Avouris P and Lyo I W 1994 *Science* **264** 942
Bürgi L, Jeandupeux O, Hirstein A, Brune H and Kern K 1998 *Phys. Rev. Lett.* **81** 5370
[4] Ortega J E *et al* 2000 *Phys. Rev. Lett.* **84** 6110
[5] Ortega J E *et al* 2001 *Surf. Sci.* **482–485** 764
[6] Mugarza A *et al* 2001 *Phys. Rev. Lett.* **87** 107601

[7] Baumberger F, Greber T and Osterwalder J 2001 *Phys. Rev.* B **64** 195411
[8] Ortega J E *et al* 2002 *Phys. Rev.* B **65** 165413
[9] Mugarza A *et al* 2002 *Phys. Rev.* B **66** 245419
[10] Mugarza A, Ortega J E, Himpsel F J and García de Abajo F J 2003 *Phys. Rev.* B **67** 081404
[11] Mugarza A and Ortega J E 2003 *J. Phys.: Condens. Matter* **15** S3281
[12] Baumberger F *et al* 2004 *Phys. Rev. Lett.* **92** 016803
[13] Baumberger F *et al* 2004 *Phys. Rev. Lett.* **92** 196805
[14] Hansmann M, Pascual J I, Ceballos G, Rust H P and Horn K 2003 *Phys. Rev.* B **67** 121409
[15] Morgenstern K, Braun K F and Rieder K H 2002 *Phys. Rev. Lett.* **89** 226801
[16] Eder R and Winter H 2004 *Phys. Rev.* B **70** 085413
[17] Lobo J *et al* 2004 *Phys. Rev. Lett.* **93** 137602
[18] Shikin A M *et al* 2004 *Phys. Rev. Lett.* **93** 146802
[19] Kevan S D 1983 *Phys. Rev.* B **28** 2268
[20] Schiller F, Halilov S V and Laubschat L 2003 *Phys. Rev.* B **67** 214431
[21] Courths R and Hüfner S 1984 *Phys. Rep.* **112** 53